

# The Mechanical Behaviour of Clay Shales and Implications on the Design of Tunnels

By

**M. Bonini, D. Debernardi, M. Barla, G. Barla**

Department of Structural and Geotechnical Engineering,  
Politecnico di Torino, Torino, Italy

Received January 8, 2007; accepted July 4, 2007  
Published online October 9, 2007 © Springer-Verlag 2007

## Summary

This paper is a contribution to the study of tunnelling in difficult conditions, with attention paid to large time-dependent deformations, which may develop either during construction, causing instabilities of the tunnel heading and of the face, or during the service life of the tunnel. Under these circumstances the construction costs may rise due to the delays in excavation time, the stabilisation and heavy support measures that need be adopted. Following a review of characterisation and modelling of time-dependent behaviour in rock, the mechanical behaviour of Clay Shales (CS), a structurally complex formation of the Apennines (Italy), is described. Then, the key factors involved in the selection of the constitutive model for CS are identified. Two constitutive models are selected and discussed and their specific material parameters determined. A case study of a large size tunnel is presented where numerical modelling by the finite difference method is carried out. The results of modelling are compared with the monitoring data in terms of radial convergence of the tunnel and extrusion of the tunnel face.

*Keywords:* Constitutive laws, numerical modelling, clay shales, time-dependent behaviour, tunnelling.

## List of Symbols

$a$	constitutive parameter
$c$	cohesion
$c_v$	primary consolidation coefficient
$E$	Young's modulus
$e_{ij}$	deviatoric strain tensor
$\dot{e}_{ij}$	deviatoric strain rate tensor
$F$	overstress function
$f$	yield function
$F_0, f_0$	stress reference unit
$\bar{f}$	part of the yield function dependent on the stress state
$G^K$	Kelvin shear modulus

$G^M$	Maxwell shear modulus
$g$	potential function
$J_{2, \text{ep}}$	second invariant of the viscoplastic strain deviator
$K$	swelling coefficient, bulk modulus
$k$	hydraulic conductivity
$m$	constitutive parameter
$n$	constitutive parameter
$p$	mean stress
$p_0$	initial state of stress
$q$	deviator
$R_{eq}$	equivalent radius
$s$	2D mean stress
$s_{ij}$	deviatoric stress tensor
$\dot{s}_{ij}$	deviatoric stress rate tensor
$t$	2D deviator, time
$\alpha$	constitutive parameter
$\beta$	constitutive parameter
$\Delta, \Delta'$	gap
$\delta_{ij}$	Kronecker delta
$\varepsilon_a$	axial strain
$\varepsilon_a^{\text{creep}}$	creep axial strain
$\dot{\varepsilon}_a$	axial strain rate
$\varepsilon_{ij}$	strain tensor
$\dot{\varepsilon}_{ij}$	strain rate tensor
$\varepsilon_{kk}$	first strain invariant
$\varepsilon_r$	radial strain
$\varepsilon_{\text{vol}}$	volumetric strain
$\varepsilon_{\text{vp}}$	equivalent visco-plastic strain
$\Phi$	viscous nucleus
$\phi$	friction angle
$\gamma$	constitutive parameter
$\eta^K$	Kelvin dynamic viscosity
$\eta^M$	Maxwell dynamic viscosity
$\kappa$	part of the yield function dependent on the viscoplastic strain rate
$\lambda$	plastic multiplier
$\nu$	Poisson's ratio
$\sigma_a$	axial stress
$\sigma_{ij}$	stress tensor
$\sigma_{kk}$	first stress invariant
$\sigma_r$	radial stress
$\sigma_t$	tensile strength
$\chi$	parameter
$\psi$	dilation angle

## 1. Introduction

The construction of large size tunnels in rocks which exhibit a time-dependent behaviour often involves operational difficulties in relation to the stability of the tunnel heading and of the face, mainly in connection with conventional full face excavation (Barla, 2006). In such cases, special care must be taken of many design aspects, with respect to the choice of the stabilisation measures and the construction sequences to be adopted.

When time-dependent deformations are accompanied by the presence of rock masses with a complex structure, the necessity of understanding the most important features of the mechanical behaviour rises in connection with the importance of finding a reliable approach for predicting the tunnel response to excavation. Laboratory testing, monitoring and numerical modelling are fundamental components of a comprehensive design approach.

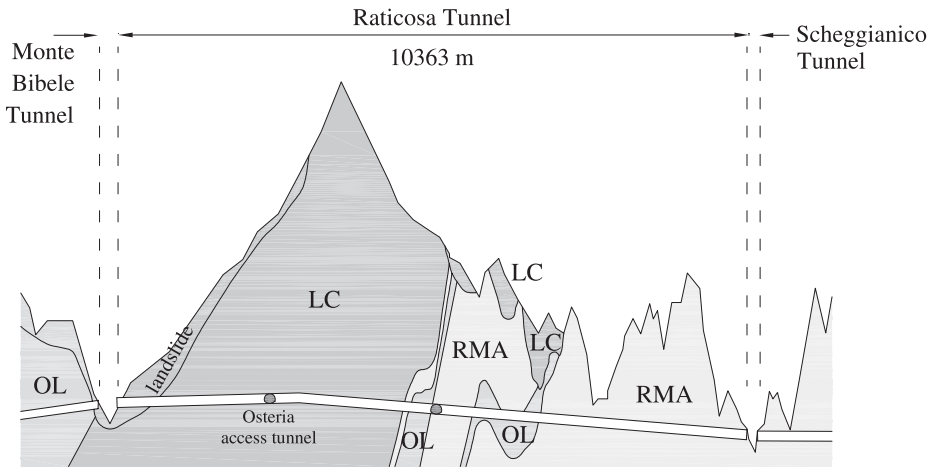


**Fig. 1.** Longitudinal section of the Raticosa tunnel: *LC* Chaotic Complex Clay-Shales; *OL* Olistostromes; *RMA* marly formations and sandstones

This paper investigates the mechanical behaviour of the Apennines Clay Shales (CS), pertaining to the so called Chaotic Complex. The aim is to identify the key factors influencing such a behaviour and to assess the relations between laboratory testing, monitoring and numerical modelling of tunnel excavation. The case study presented (Fig. 1) is part of the Italian High Speed Railway project, between Bologna and Firenze (Lunardi and Focaracci, 1999). The presence of CS, which exhibit squeezing and/or swelling behaviour, associated with the morphologic characteristics of the Apennines, may lead to serious difficulties in tunnel construction.

## 2. Review of Characterisation and Modelling

Clay Shales (CS) cannot be confidently studied and modelled with the classical approaches of Soil and Rock Mechanics. Common in many countries, in Italy they are mostly Meso-Cenozoic, deformed by the Alpidic orogenesis (A.G.I., 1979).

### 2.1 Characterisation

CS are usually the result of depositional or post-depositional events of physical, chemical or tectonic origin and pertain to formations outcropping along the Apennines, which sedimented some tens millions years ago in a marine environment due to turbid flows at the base of the continental shelf. Their main characteristics depend on the shape of the basin, the subsiding period and the nature and grading of terrigenous contribution.

During the last decades many factors have been widely investigated in order to understand the implications on the mechanical behaviour of CS. Depositional events (marine/continental environment), chemical (pore fluid composition, bonding or ce-

mentation), climatic conditions (glaciations) and tectonics (large scale movements, landslides) are the most significant. The effects of these factors act by modifying structure, texture, porosity, fissure pattern and grain size distribution. Only the fundamental aspects are considered in the following.

The term Clay Shales has been used with many meanings, such as presence of bonding between particles or aggregates (Leroueil and Vaughan, 1990), or arrangement of particles, particle groups and pore spaces (Mitchell and Soga, 2005). In general, the term itself should be preferably used to imply the combined effects of fabric, composition and inter-particle forces. The classification of CS given by A.G.I. (1979) has been recently refined by Picarelli et al. (2000) who introduced a connection between structure and behaviour at laboratory and field scale. It has been shown that weathering, cycles of wetting and drying and stress release induce further changes to the structure of CS (D'Elia, 1980; Cicoella and Picarelli, 1990).

In CS, the grain size distribution obtained by conventional methods does not usually reflect the real content of clay minerals (A.G.I., 1979). The soil matrix is generally made of fragments of hard clays, which may form bonded aggregates. Few cycles of wetting and drying determine a significant reduction of the fragments size (Picarelli and Olivares, 1998). Consequently, the index properties and the Atterberg limits of CS are quite variable. Several studies, on compressibility, state boundary surfaces, and swelling behaviour of CS have started from the adoption of the reconstituting technique due to Burland (1990), thus introducing a debate on the appropriate reference material for characterisation.

The influence of physical-chemical interactions on CS was addressed by performing ion diffusion experiments during compression/swelling oedometer tests. Different pore liquids were employed for this purpose. The first results showed that all the clay minerals present in CS are sensitive to pore fluid composition, though the extent and the way of response may change from case to case (Di Maio and Fenelli, 1997).

## 2.2 Modelling

There is clear evidence in laboratory testing of CS that they often show a time-dependent behaviour (D'Elia, 1991; Bonini, 2003), which develops in the form of swelling or squeezing behaviour. The first models used to describe the swelling behaviour are a direct consequence of the frameworks in which are embedded the experimental tests used to identify and quantify the phenomenon. For instance, Grob's law (Huder and Amberg, 1970; Grob, 1972) and the early developments due to Wittke (1978) and Pregl et al. (1980) follow respectively from the results of the Huder-Amberg swelling tests, applied to either one- or three-dimensional swelling laws, and multi-axial tests.

The choice of other possible physical-chemical-mechanical processes as a basis of the phenomenon brought modelling developments away from the pure laboratory evidence. Laboratory testing was still a basic ingredient, at least for parameter determination and law validation, but was not the exclusive component of the constitutive models developed. Models of this type are due to Wittke (2000), Gysel (2002),

Bellwald (1990), Aristorenas (1992) and Einstein (2000). Anagnostou (1991, 1995) introduced a continuum-mechanical stress-analysis-based model where swelling is described as a coupled hydraulic-mechanical process, taking into account the influence of saturation on hydraulic conductivity.

According to Alonso et al. (1999), the behaviour of unsaturated expansive clays is closely associated with the mechanical and physical-chemical phenomena occurring at particle level, which are a consequence of the properties of the active clay minerals contained in the soil. Loret et al. (2002) developed a model based on the mixture-theory approach introduced in the study of clay barriers and petroleum drilling according to which water in nano-pores ( $<10^{-9}$  m) corresponding to the size of clay interstices has properties very different from the properties of bulk water. The models due to Pimentel (1996) and Wong (1998) take into account the reduction of water content, shear strength and stiffness involved in the process of swelling.

Whatever may be the classification of the model used (total/effective stresses, micro/macro-scale, phenomenological/mechanistic), a model of the swelling behaviour should not lack of the following features: a coupled framework considering effective stresses and experimentation based on the use of triaxial tests, which allow for the consideration of real boundary and stress history conditions.

The models developed for simulating the squeezing conditions generally aim at focusing on the creep behaviour dependent or independent of the mobilised stress level, damage and/or failure (Barla, 2001). The most simple and frequent creep laws contain time as explicit variable (explicit time functions) and derive from direct observation of experimental data. They include primary and secondary creep laws.

Otherwise, implicit time functions include visco-elastic (Maxwell's linear and Kelvin-Voigt's, Burgers' or Zener's non linear models) and visco-elastic-plastic analogical models (for example, obtained summing up a visco-elastic Burgers model with the Mohr-Coulomb yield criterion) where the creep component is independent of failure. Recently, more complex elasto-visco-plastic models have been proposed with the intent of modelling also tertiary creep as a function of stress and strain level (Gioda and Cividini, 1996).

The most advanced and recent visco-plastic models are formulated on the basis of potential laws (Olszak and Perzyna, 1964; Perzyna, 1966; Lemaitre and Chaboche, 1996), which associate plasticity theory to recent studies of rheological phenomena. These elasto-visco-plastic models differ from the elasto-plastic models for the definition of possible states out of the yield surface, that is  $df > 0$ . It is therefore impossible to determine the plastic flow law through the consistency condition.

The above models have both advantages and disadvantages. The rheological models assume that time-dependent deformations derive from the material viscous nature. Most of them lack the component related to volumetric deformation and time-dependent phenomena accompanied by moisture changes are neglected. The advantage of using a rheological model is that, since parameters are derived from measured data, the model will correctly simulate the observed behaviour. The applicability of the model to other cases is however uncertain. Rheological parameters should be treated like material parameters; this implies the use of systematic and economical ways to conduct laboratory and in-situ tests to derive the parameters.

On the other hand, potential laws allow for the consideration of a more wide concept which groups elasto-plastic and visco-elasto-plastic laws in the same framework. The effective stress principle is taken into account. Although theoretically appealing, potential laws introduce the problem (common to complex rheological models) of determining not physically based model parameters.

### 3. Geotechnical Characterisation of Clay-Shales

The specimens involved in this study (a description of the site is given in Sect. 5.) were retrieved from cubic samples cut directly from the tunnel face (Fig. 2), at chainage 116 m (22 m depth) in the Raticosa tunnel (landslide area) and at chainages 590 m and 620 m (140 m depth) in the Osteria access adit. Considering the presence of lithic components such as calcareous, marly and sandstone blocks in the form of disarranged



**Fig. 2.** Typical block taken from the tunnel face

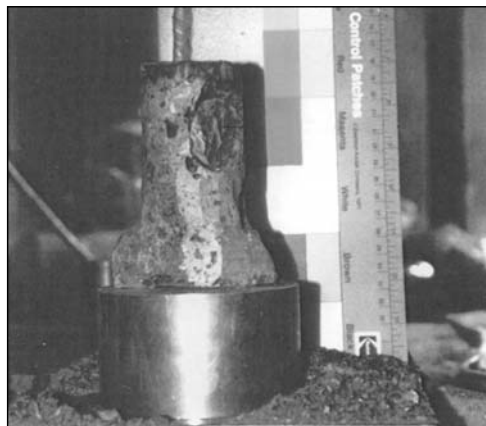


**Fig. 3.** Specimen preparation

elements, cylindrical specimens (to be used in laboratory tests) were obtained with great difficulty (Fig. 3). The material in excess was used to determine the physical properties and the mineralogical composition and to perform oedometer tests on reconstituted material.

### 3.1 Physical and Mineralogical Properties

The grain size distribution proved to be variable; silt and sand may be present, although most significant is the presence of clay particles. According to the Plasticity Chart, the CS are classified as “inorganic clays of low to average plasticity”. Table 1 shows the physical properties. Based on X-ray diffraction analyses the clay fraction is more than 50%. As the clay content evaluated from the grain size distribution is less than this quantity, one can infer that some of the larger particles (more than 0.002 mm in diameter) are made of attached clay grains. The remaining minerals are quartz, calcite and albite (in traces). The clayey minerals reported in Table 2 are listed by decreasing Cation Exchange Capacity (decreasing swelling potential). The CS contain expandable minerals in ratio of 20–50% of the total of the clay minerals.

The hydraulic conductivity is influenced by a two-fold aspect: the clay matrix exhibits a very low permeability and the close network of fissures which are present contributes significantly to the overall hydraulic conductivity. At shallow depth these fissures may have a considerable influence, while the natural water content (5–22%), as well as the degree of saturation (80–98%), increases with the overburden. The values of the primary consolidation coefficient  $c_v$  and of the hydraulic conductivity  $k$  calculated from the oedometer tests are in the range  $1 \times 10^{-7}$ – $1 \times 10^{-8}$  m<sup>2</sup>/sec and  $1 \times 10^{-9}$ – $1 \times 10^{-12}$  m/sec, respectively. From the oedometer tests performed on natural and reconstituted materials, it is shown that the hydraulic conductivity is strictly dependent on the void index even if the structure is essentially different. This means that, at least at the sample scale, the fissures have a negligible influence on hydraulic conductivity.

**Table 1.** Physical properties of the CS\*

Tunnel	$\gamma_d$ (kN/m <sup>3</sup> )	$G_s$ (–)	$w_n$ (%)	$LL$ (%)	$PL$ (%)	$PI$ (%)
Raticosa	20.5	2.7	11.5	40–43	21–22	≈ 20
Osteria	21.7	2.7	7.0	34–43	18–20	14–25

\*  $\gamma_d$  drained unit weight;  $G_s$  specific weight;  $w_n$  natural water content;  $LL$  liquid limit;  $PL$  plastic limit;  $PI$  plastic index

**Table 2.** Results of the X-ray diffraction analyses

Soil	Smectite (%)	Illite (%)	Illite-Smectite (%)	Chlorite (%)	Kaolinite (%)
Raticosa	5	25–50	10–20	40–50	–
Osteria (sample 1)	5	20–40	10–25	30–40	–
Osteria (sample 2)	5–10	10–25	25–50	30–40	–
Osteria (sample 3)	5–15	5–20	25–50	20–30	–

3.2 Swelling Properties

The swelling potential of CS is well illustrated in Fig. 4. Each point in the triangular plot is defined by three percentages of clay minerals, quartz and carbonate content, respectively, as shown clockwise from 0 to 100%. The diagram does not account for the effective amount of swelling shown by the different clay minerals (smectite, illite, etc.). An average to high swelling potential is shown to characterize the CS. The swelling potential has also been investigated by means of the Huder-Amberg modified oedometer test (Madsen, 1999). This allows for the determination of the swelling coefficient  $K$  (4.1% for Raticosa tunnel, 4.9–10.6% for Osteria access adit) on the diagram giving the vertical strain versus the effective vertical stress as shown in Fig. 5.

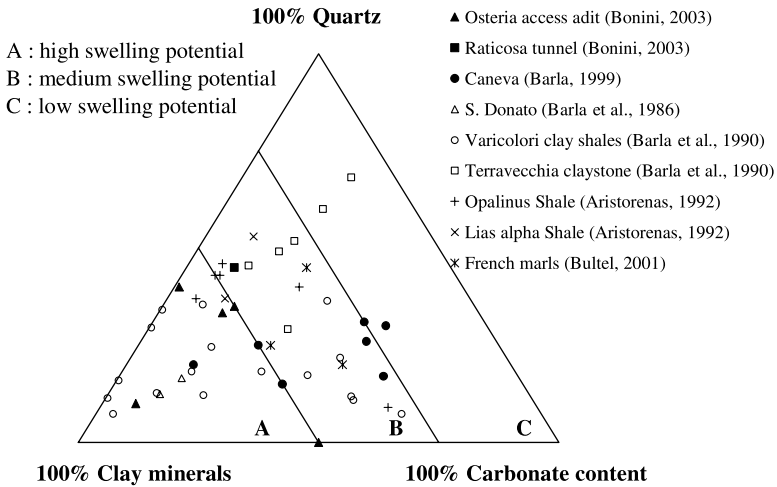


Fig. 4. Swelling potential of CS compared to other rocks

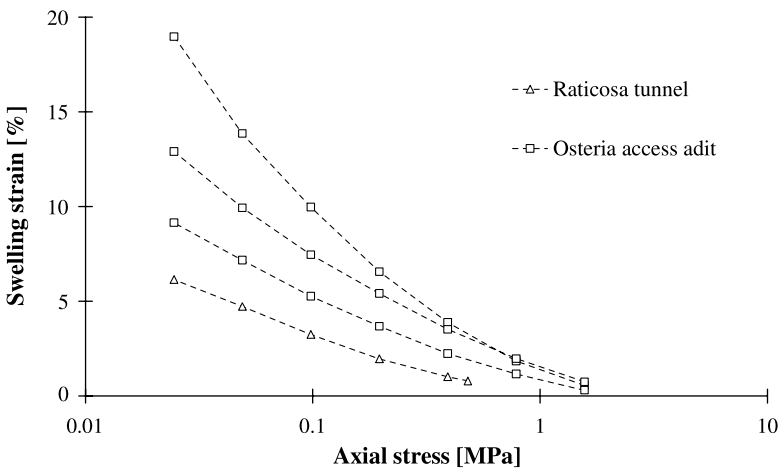


Fig. 5. Results of swelling tests

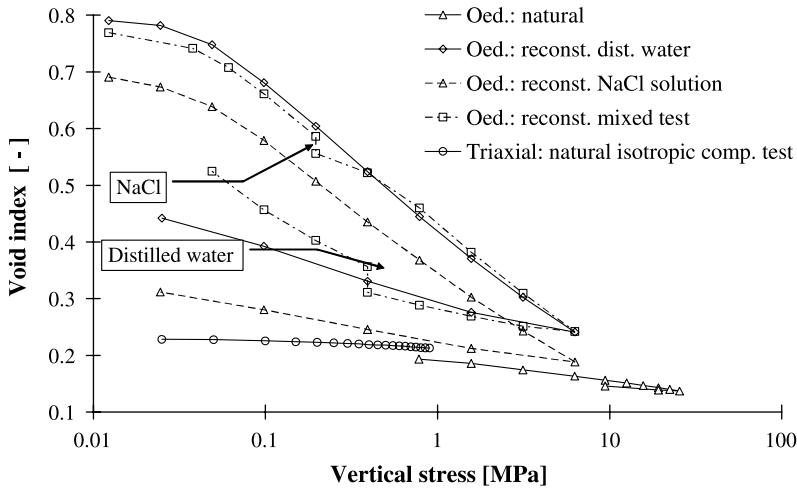


Fig. 6. Compression curves from oedometer and triaxial tests

The compressibility characteristics of CS may be inferred by comparing the results of oedometer tests on natural and reconstituted samples, which allow for the determination of the influence of structure and material intrinsic properties. For the purpose of this study, the natural material was remoulded with a pestle and sieved through the ASTM sieves nr. 10 and 40. Aggregates included in the matrix were thus separated from the rest. The materials were mixed at a water content equal to 1.5 the liquid limit. Moreover, the chemical composition of the pore fluid was changed (i.e. adding NaCl and vice versa) in order to check the sensitivity of expandable minerals (Fig. 6). Chemical consolidation and swelling were induced and the swelling index determined to be a function of cation concentration. The swelling strain obtained during exposure to distilled water (higher than the consolidation strain due to exposure to NaCl solution at the same load) may be due to a decrease of the pore fluid ionic concentration to a value lower than the initial one.

### 3.3 Mechanical Behaviour

Triaxial tests in closely controlled stress-path conditions are a useful tool for the simulation of the tunnel short- and long-term behaviour at laboratory scale. With

Table 3. Triaxial tests performed\*

Test	Type	$B$ (-)	$b.p.$ (kPa)	$\sigma'_c$ (kPa)	$\dot{\epsilon}_a$ (mm/min)	$t_{\max}$ (kPa)	$s'_{\max}$ (kPa)	$\Delta u$ (kPa)
OST3	CID	-	0	900	0.0005	538	1438	-
RTC1	CIU	0.81	400	486	0.001	170	555	-65
RTC2	CIU + cr	0.75	403	496	0.01	181	524	-28
RTC3	CIU + cr	0.77	399	497	0.005	148	480	18
RTC4	CIU + cr	0.80	404	488	0.005	94	453	31
RTC5	CIU + cr + dr	0.65	396	501	0.001	134	491	9

\*  $B$  Skempton's parameter;  $b.p.$  back pressure;  $\sigma'_c$  consolidation effective stress;  $\dot{\epsilon}_a$  axial strain rate in the shearing phase;  $t_{\max} = (\sigma_v - \sigma_h)_{\max}/2$ ;  $s'_{\max} = (\sigma'_v + \sigma'_h)_{\max}/2$ ;  $\Delta u$  excess pore pressure

reference to the Raticosa tunnel, a total of six triaxial tests (Table 3) were performed by means of the Soft Rock Triaxial Apparatus (SRTA) available at the DIPLAB (Disaster Planning LABORatory) of Politecnico di Torino. The aim was to simulate at laboratory scale the tunnel behaviour in short and long term conditions.

The testing procedure adopted for triaxial testing was designed for the characterisation of soft rocks showing swelling behaviour and/or subjected to squeezing conditions (Barla, 1999). It consists of seven phases: the sample preparation is carried out with great care in order to avoid any possible disturbance. The flushing phase is to saturate the dry back-pressure circuit, preventing swelling due to the contact with water. The saturation of the specimen takes place by a step by step increase of back-pressure and the degree of saturation is controlled during each step by evaluation of



Fig. 7. Typical specimen after failure

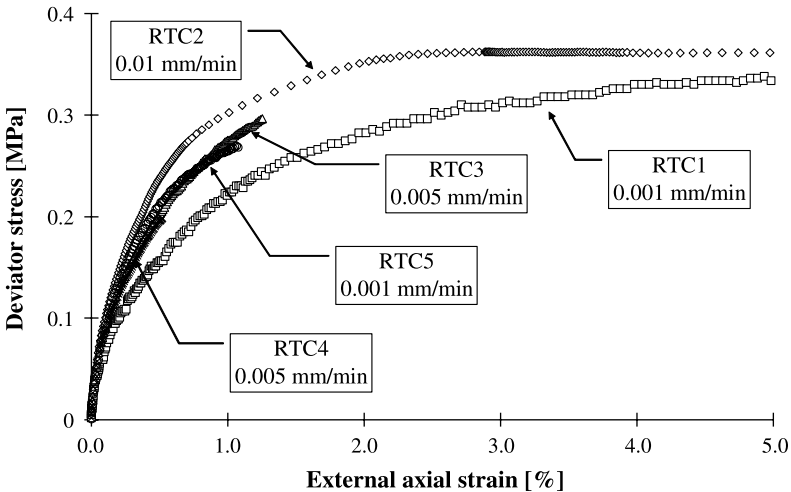


Fig. 8. Stress–strain behaviour for different axial strain rates

**Table 4.** Strength parameters (mean values)\*

Tunnel	$c_u$ (kPa)	$c'_p$ (kPa)		$c'_r$ (kPa)		$\varphi'_p$ (°)		$\phi'_r$ (°)	
		TX	DS	TX	DS	TX	DS	TX	DS
Raticosa	100–900	16–540		15	20	16	–	16	–
Osteria	–	48	23	15	20	29	22	17	7

\*  $c_u$  undrained shear strength;  $c'_p$ ,  $c'_r$  peak and residual cohesion;  $\varphi'_p$ ,  $\phi'_r$  peak and residual friction angle

the Skempton's pore pressure parameter. The consolidation phase brings the specimen to its original stress conditions. Once the desired conditions are attained, stresses are maintained constant for the time required to reach a creep rate lower than 0.05%/day.

At this point the specimens were subjected to  $s = (\sigma_1 + \sigma_3)/2$  constant stress path, typical of an element of ground located at the tunnel sidewall. A typical failure surface in the specimen is shown in Fig. 7. The stress–strain curves obtained for the Raticosa tunnel (Fig. 8) exhibit a hyperbolic behaviour, influenced by the rate of axial displacement and saturation degree. The strength parameters inferred from both triaxial (TX) and direct shear (DS) tests are shown in Table 4.

Once the desired mobilised deviatoric stress level is reached, the sample is subjected to a constant stress level until a creep level lower than  $\dot{\epsilon}_a \leq 0.05\%$ /day is attained. Since the short-term behaviour near the tunnel face is expected to be undrained, the drainage is still closed. During this phase, the sample exhibits a time-dependent behaviour as shown by the strain rate versus time plots under deviatoric loading (Fig. 9). Time-dependent strains develop for a mobilised strength nearly equal to 50% of the failure value. Moreover, the strain rate is shown not to increase significantly as the stress increases.

Finally, the drainage is opened in order to simulate the drained conditions which occur around the tunnel in the case of a standstill or as face advance takes place. Due

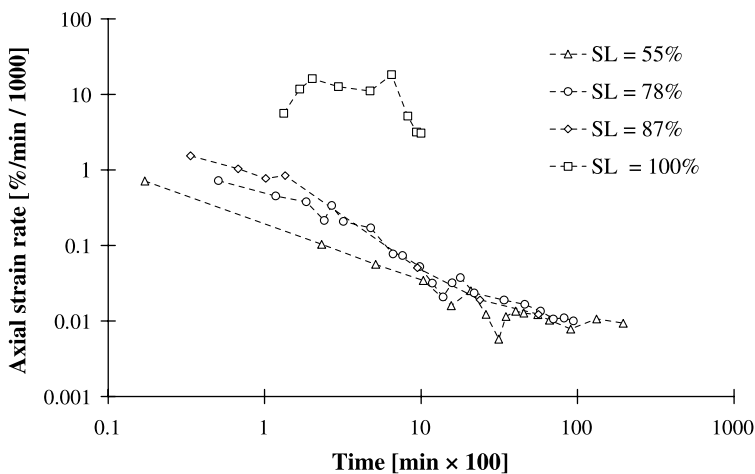


**Fig. 9.** Axial strain rate versus time obtained for different stress levels (SL)

to the difficulties associated with the creep phase, only the RTC5 specimen was subject to the drained phase (Table 3), which was very difficult to interpret. The difficulties lay mostly in the superimposition of various effects like mechanical swelling due to stabilisation of pore pressure, to the beginning of chemical swelling as a consequence of water ingress and to unavoidable creep strains.

### 3.4 Discussion

Oedometer tests performed on natural and reconstituted samples evidence the very low void index of the natural samples and the sensitivity to the ionic concentration of the pore fluid for the reconstituted samples. The swelling potential is from average to high, with magnitudes as shown by other Clay Shales (see: Bonini et al., 2003; Barla et al., 2004 for more details).

Triaxial tests performed in closely controlled conditions exhibit an isotropic behaviour. It is not possible to determine a unique effective stress path for the performed tests. The effective stress path is dependent on the saturation degree and on the axial strain rate. The strength parameters are generally influenced by particle arrangement and orientation of discontinuities, saturation degree, loosening and stress release due to sampling, etc. Failure in TX tests often takes place along planes on which fragments tend to align. The strength parameters are influenced by the direction of shearing.

During the creep tests and during the creep phases of the triaxial tests, most of the samples under deviatoric loading exhibit significant time-dependent strains. The time-dependent behaviour is shown to be present also at low stress level. In particular, during the drained phase of the RTC5 test (Table 3), mechanical swelling, chemical swelling and creep are shown to occur simultaneously.

The following conclusions can be drawn:

- when time-dependent strains are negligible, the Mohr-Coulomb yield criterion can be used with confidence;
- the hydraulic conductivity and the natural water content are very low. Notwithstanding the presence of swelling minerals, the on-set of swelling is prevented, at least in the short-term. It is expected that CS undergo a time-dependent behaviour.

## 4. Time-Dependent Constitutive Models

On the basis of the evidences highlighted during laboratory tests (low water permeability, high inelastic and viscous strains), two constitutive models have been used to simulate the mechanical and time-dependent behaviour of CS: a viscoelastic-plastic model (CVISC) and an elastic-viscoplastic model (VIPLA).

### 4.1 Visco-Elastic-Plastic Model (CVISC)

The CVISC model (Itasca, 2001) is an analogical model which couples, in series, the Burgers viscoelastic model with a plastic flow rule, based on the Mohr-Coulomb yield

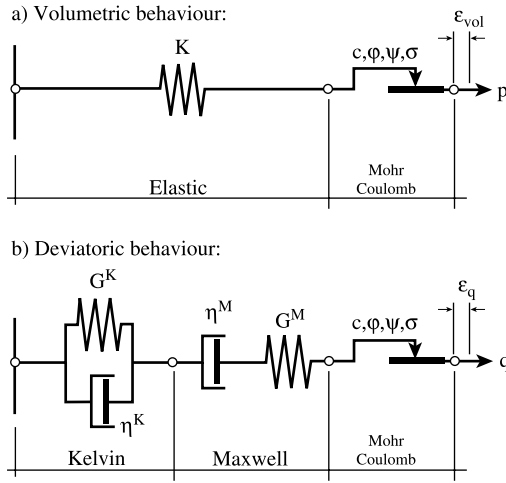


Fig. 10. Sketch of the CVISC model

criterion, as shown in Fig. 10. The main assumption of this model is to split the mechanical behaviour of the material into volumetric and deviatoric components. In terms of strain and stress, one writes:

$$\varepsilon_{vol} = \varepsilon_{kk} \quad \text{and} \quad \varepsilon_{vol} = \varepsilon_{vol}^e + \varepsilon_{vol}^p \quad (1)$$

$$e_{ij} = \varepsilon_{ij} - \delta_{ij} \cdot \frac{\varepsilon_{vol}}{3} \quad \text{and} \quad e_{ij} = e_{ij}^{ve} + e_{ij}^p \quad (2)$$

$$p = \frac{\sigma_{kk}}{3} \quad (3)$$

$$s_{ij} = \sigma_{ij} - \delta_{ij} \cdot p \quad (4)$$

The volumetric behaviour is only elasto-plastic and is governed by the linear elastic law and the plastic flow rule (Fig. 10a), while the deviatoric behaviour is viscoelastic-plastic and is driven by the Burgers model and the same plastic flow rule (Fig. 10b). This means that the viscoelastic strains are deviatoric and depend only on the deviatoric stress  $s_{ij}$ , instead the plastic strains are both deviatoric and volumetric and depend on  $\sigma_{ij}$  in accordance with the chosen flow rule.

The viscoelastic part can be described by the following relations, which hold true for the Kelvin element (superscript  $K$ ) and for the Maxwell element (superscript  $M$ ), respectively (these relations form, in series, the Burgers model):

$$e_{ij}^{ve} = e_{ij}^{veK} + e_{ij}^{veM} \quad (5)$$

$$\text{Kelvin element:} \quad s_{ij} = 2G^K e_{ij}^{veK} + 2\eta^K \dot{e}_{ij}^{veK} \quad (6)$$

$$\text{Maxwell element:} \quad \dot{e}_{ij}^{veM} = \frac{\dot{s}_{ij}}{2G^M} + \frac{s_{ij}}{2\eta^M} \quad (7)$$

The plastic strains follow the general flow rule of plasticity:

$$\varepsilon_{ij}^p = \lambda \cdot \frac{\partial g}{\partial \sigma_{ij}} \quad (8)$$

$$\varepsilon_{\text{vol}}^p = \lambda \cdot \left[ \frac{\partial g}{\partial \sigma_{11}} + \frac{\partial g}{\partial \sigma_{22}} + \frac{\partial g}{\partial \sigma_{33}} \right] \quad (9)$$

$$\varepsilon_{ij}^p = \lambda \cdot \frac{\partial g}{\partial \sigma_{ij}} - \delta_{ij} \cdot \frac{\varepsilon_{\text{vol}}^p}{3} \quad (10)$$

where  $\lambda$  is the plastic multiplier and  $g$  the plastic potential, with the same shape of the Mohr-Coulomb yield criterion, but controlled by the dilation angle  $\psi$ .

Finally, the elastic part of the volumetric behaviour is described by the relation:

$$p = K(\varepsilon_{\text{vol}} - \varepsilon_{\text{vol}}^p) \quad (11)$$

The model is characterised by nine parameters as follows: elastic properties (bulk modulus  $K$ ), viscoelastic properties (Maxwell dynamic viscosity  $\eta^M$  and shear modulus  $G^M$ , Kelvin dynamic viscosity  $\eta^K$  and shear modulus  $G^K$ ) and plastic properties (cohesion  $c$ , friction angle  $\phi$ , uniaxial tensile strength  $\sigma_t$  and dilation angle  $\psi$ ).

The constitutive parameters can be derived by means of analytical and numerical fitting of experimental data. The elastic and plastic parameters can be determined from classical deformation and strength tests following a standard procedure. The viscoelastic parameters can be derived from triaxial tests (creep, relaxation, constant strain rate tests). It is however more reliable to use creep tests.

In the case of creep tests, the main assumption is that the stress level is lower than the yield strength: without the plastic component the CVISC model reduces to the Burgers model. For a cylindrical specimen subjected to axial and radial stresses,  $\sigma_a$  and  $\sigma_r$ , the induced axial and radial viscoelastic strains,  $\varepsilon_a$  and  $\varepsilon_r$ , are:

$$\varepsilon_a = \frac{p}{3 \cdot K} + \frac{q}{3 \cdot G^M} + \frac{q}{3 \cdot \eta^M} \cdot t + \frac{q}{3 \cdot G^K} \cdot \left[ 1 - \exp\left(-\frac{G^K}{\eta^K} \cdot t\right) \right] \quad (12)$$

$$\varepsilon_r = \frac{p}{3 \cdot K} - \frac{q}{6 \cdot G^M} - \frac{q}{6 \cdot \eta^M} \cdot t - \frac{q}{6 \cdot G^K} \cdot \left[ 1 - \exp\left(-\frac{G^K}{\eta^K} \cdot t\right) \right] \quad (13)$$

Both these relations allow one to determine the required parameters by means of numerical fitting. It is observed that Eq. (12) is more suitable for this purpose, because the axial strain  $\varepsilon_a$  is in general measured in a more accurate and reliable manner. The axial creep strain  $\varepsilon_a^{\text{creep}}$  is obtained by subtracting the instantaneous elastic axial strain from the total axial strain  $\varepsilon_a$ :

$$\begin{aligned} \varepsilon_a^{\text{creep}} &= \varepsilon_a - \varepsilon_a^e = \varepsilon_a - \left( \frac{p}{3 \cdot K} + \frac{q}{3 \cdot G^M} \right) \\ &= \frac{q}{3 \cdot G^K} + \frac{q}{3 \cdot \eta^M} \cdot t + \frac{q}{3 \cdot G^K} \cdot \exp\left(-\frac{G^K}{\eta^K} \cdot t\right) \end{aligned} \quad (14)$$

Equation (14) is the sum of three terms: the first is a constant, the second is linear with time and the third tends exponentially to zero. It is necessary to find the contri-

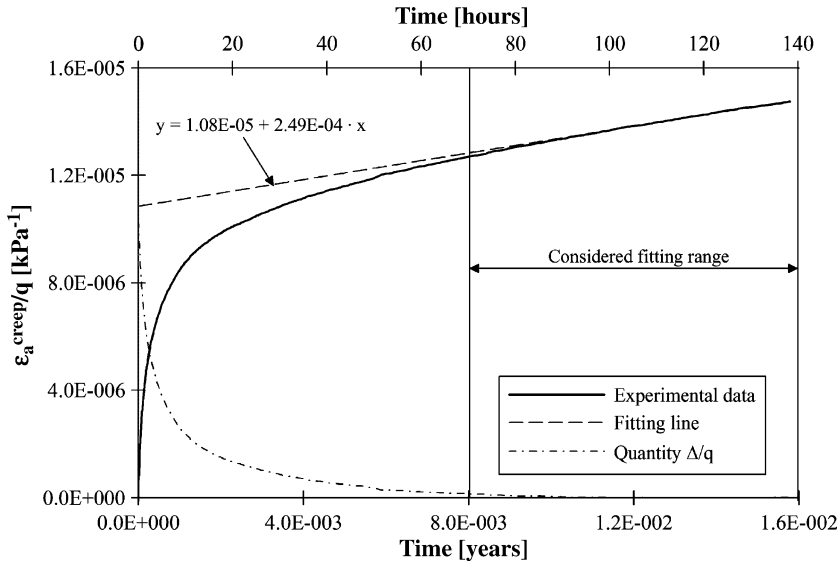


Fig. 11. Procedure for the evaluation of parameters  $\eta^M$  and  $G^K$  for the CVISC model

tribution of each term to determine the viscous parameters. The experimental data can be interpolated in a range of the creep curve where the slope is almost constant (i.e. where the contribution of the third term in Eq. (14) is practically negligible). The slope of the fitting curve is equal to  $q/(3 \cdot \eta^M)$  while its intercept is  $q/(3 \cdot G^K)$  and the parameters  $\eta^M$  and  $G^K$  can be easily derived.

This procedure is applied in Fig. 11 for typical creep tests performed on CS specimens as described above. As tests were carried out at different stress levels, the axial strain was normalized to  $q$ , deriving an average representative curve. The values obtained for  $\eta^M$  and  $G^K$  are listed in Table 5.

The parameter  $\eta^K$  can be computed by evaluating the gap  $\Delta$  between the experimental data and the linear part of Eq. (14), which is known once  $\eta^M$  and  $G^K$  are known:

$$\Delta = \varepsilon_a^{\text{creep}} - \frac{q}{3 \cdot G^K} - \frac{q}{3 \cdot \eta^M} \cdot t \cong \frac{q}{3 \cdot G^K} \cdot \exp\left(-\frac{G^K}{\eta^K} \cdot t\right) \quad (15)$$

Table 5. Parameters of the CVISC model for the Raticosa tunnel, at laboratory and in situ scale

	$c'$ (kPa)	$\phi'$ (°)	$\psi$ (°)	$\sigma'_t$ (kPa)	
Laboratory	20	16	0	5	
Tunnel	100				
	$K$ (kPa)	$G^M$ (kPa)	$G^K$ (kPa)	$\eta^M$ (kPa · year)	$\eta^K$ (kPa · year)
Laboratory	$41.7 \times 10^3$	$19.2 \times 10^3$	$30.7 \times 10^3$	1338	34
Tunnel	$866 \times 10^3$	$400 \times 10^3$		$1522 \times 10^3$	34

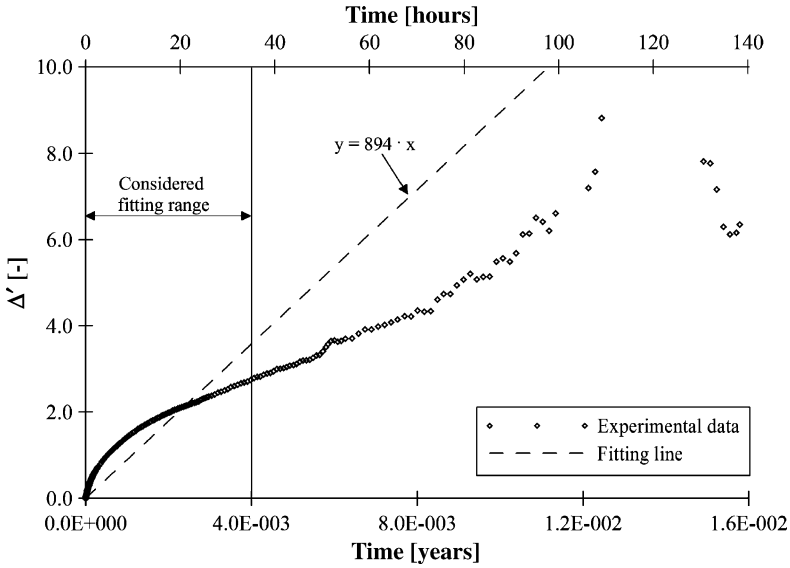


Fig. 12. Procedure for the evaluation of parameter  $\eta^K$  for the CVISC model

By dividing this equation by  $q/(3 \cdot G^K)$ , introducing the natural logarithm, and changing sign,  $\Delta'$  can be obtained:

$$\Delta' = -\ln\left(\frac{\Delta}{q/(3 \cdot G^K)}\right) \cong \frac{G^K}{\eta^K} \cdot t \quad (16)$$

The slope of the curve fitting the experimental quantity  $\Delta'$  versus time  $t$  and passing through the origin is equal to  $G^K/\eta^K$ . Then, the parameter  $\eta^K$  can be computed as shown in Fig. 12 and in Table 5.

#### 4.2 Elastic-Visco-Plastic Model (VIPLA)

The VIPLA model belongs to Perzyna's general theory of elasto-visco-plasticity, which is an extension of the classical theory of plasticity. It was originally proposed by Lemaitre and Chaboche (1996) for metal alloys and extended by Pellet et al. (2005) to the study of the time-dependent behaviour of rocks. The model has been shown to be in good agreement with both laboratory and in situ data derived for claystone (Boidy, 2002).

According to the theory of elasto-visco-plasticity, the strain rate tensor  $\dot{\epsilon}_{ij}$  can be split into elastic  $\dot{\epsilon}_{ij}^e$  and visco-plastic  $\dot{\epsilon}_{ij}^{vp}$  components to give:

$$\dot{\epsilon}_{ij} = \dot{\epsilon}_{ij}^e + \dot{\epsilon}_{ij}^{vp} \quad (17)$$

The visco-plastic strain rate tensor  $\dot{\epsilon}_{ij}^{vp}$  can be derived by the general flow rule:

$$\dot{\epsilon}_{ij}^{vp} = \gamma \cdot \Phi(\langle F \rangle) \cdot \frac{\partial g}{\partial \sigma_{ij}} \quad (18)$$

where  $\gamma$  is a viscous constitutive parameter,  $F$  is an over-stress function representing the distance from the yield surface  $f = 0$ ,  $\Phi(\langle F \rangle)$  is the so-called viscous nucleus,  $g$  is the visco-plastic potential and  $\sigma_{ij}$  the stress tensor.

The time-dependency is introduced by modifying the classical flow rule of plasticity and by discarding the consistency rule ( $df = 0$ ,  $f \leq 0$ ), thus allowing the yield function  $f$  to be positive or negative. The visco-plastic potential  $g$  defines the direction of  $\dot{\varepsilon}_{ij}^{vp}$ , while  $F$  influences its modulus by means of the viscous nucleus  $\Phi$ .

In the VIPLA model  $\Phi$  is assumed to be a power law and  $F$  to be represented by the yield function  $f$ :

$$\Phi(\langle F \rangle) = \left\langle \frac{F}{F_0} \right\rangle^n = \left\langle \frac{f}{f_0} \right\rangle^n, \quad n \geq 1 \quad (19)$$

where  $F_0$ ,  $f_0$  is the stress reference unit and  $n$  is a constitutive parameter.

The yield function  $f$  is splitted into a part  $\bar{f}$ , which depends only on the stress state, and a part  $\kappa$ , which depends only on the visco-plastic strain rate, according to:

$$f = \frac{\bar{f}(\sigma_{ij})}{\kappa(\dot{\varepsilon}_{ij}^{vp})} \quad (20)$$

For the function  $\bar{f}$  a Von Mises's yield criterion is assumed:

$$\bar{f}(\sigma_{ij}) = q \quad (21)$$

A potential hardening is introduced by means of the function  $\kappa$ :

$$\kappa(\dot{\varepsilon}_{ij}^{vp}) = \varepsilon_{vp}^{-m/n} \quad (22)$$

where  $m$  is a constitutive parameter ( $1 - n < m \leq 0$ ) and  $\varepsilon_{vp}$  is the so-called equivalent visco-plastic strain,  $\varepsilon_{vp} = \sqrt{4/3 \cdot J_{2,\varepsilon^{vp}}}$ , where  $J_{2,\varepsilon^{vp}}$  is the second invariant of the visco-plastic strain deviator.

Under these assumptions, the yield surface  $f = 0$  is reduced to the hydrostatic axis and it does not change with time. The visco-plastic potential  $g$  is supposed to be equal to  $\bar{f}$  (i.e. the flow rule is associated). With these assumptions, the visco-plastic strains depend on the deviatoric state only and do not induce volumetric strains. Therefore, Eq. (18) becomes:

$$\dot{\varepsilon}_{ij}^{vp} = \frac{3}{2} \cdot \gamma \cdot q^{n-1} \cdot \varepsilon_{vp}^m \cdot s_{ij} \quad (23)$$

The constitutive parameters  $n$  and  $m$  define, respectively the dependence of the visco-plastic strain rate tensor on the deviatoric stress and on the equivalent visco-plastic strain, whereas the parameter  $\gamma$  defines the amplitude of the visco-plastic strains. Equation (23) results in a closed-form solution only when  $q$  is constant; otherwise a numerical method is required.

The visco-plastic parameters can be derived by fitting of the experimental data. The most reliable and simple technique is to use the results of triaxial creep tests performed at different stress levels. During creep tests the deviatoric stress  $q$  is constant with time and Eq. (23) can be solved analytically. For a cylindrical specimen subjected to axial and radial stresses,  $\sigma_a$  and  $\sigma_r$ , the solution is:

$$\varepsilon_{vp} = a \cdot q^\beta \cdot t^\alpha \quad \text{with:} \quad \alpha = \frac{1}{1-m}; \quad \beta = \frac{n}{1-m} = n \cdot \alpha; \quad a = \left( \frac{\gamma}{\alpha} \right)^\alpha \quad (24)$$

with  $q = \sigma_a - \sigma_r$  and  $\varepsilon_{vp} = \varepsilon_a^{vp} = -1/2 \cdot \varepsilon_r^{vp}$ . Equation (24) can be written in logarithmic form, to obtain the following linear relations:

$$\ln(\varepsilon_{vp}) = \ln(\chi) + \alpha \cdot \ln(t) \quad \text{with: } \chi = a \cdot q^\beta \quad \text{and} \quad \ln(\chi) = \ln(a) + \beta \cdot \ln(q) \quad (25)$$

For each test considered, the parameter  $\alpha_i$  is defined as the slope of the line obtained by interpolation of the experimental data on the plane  $\ln(\varepsilon_{vp}) - \ln(t)$ . The parameter  $\alpha$  is chosen as the arithmetic mean of all the parameters  $\alpha_i$ . Figure 13 shows this procedure as adopted for CS. The value of  $\alpha$  is reported in Table 6. Then, for each test the experimental curve  $\varepsilon_{vp} - t$  is normalized with respect to  $t^\alpha$  and the parameter  $\chi_i$  is assumed to be the arithmetical mean of the curve obtained.

The parameters  $\beta$  and  $a$  are selected as the slope and the natural exponential of the intercept with the y-axis of the linear interpolation of the couples  $\chi_i - q_i$  evaluated for each test, on the plane  $\ln(\chi_i) - \ln(q_i)$ . Finally, the parameters  $\gamma$ ,  $m$  and  $n$  are derived

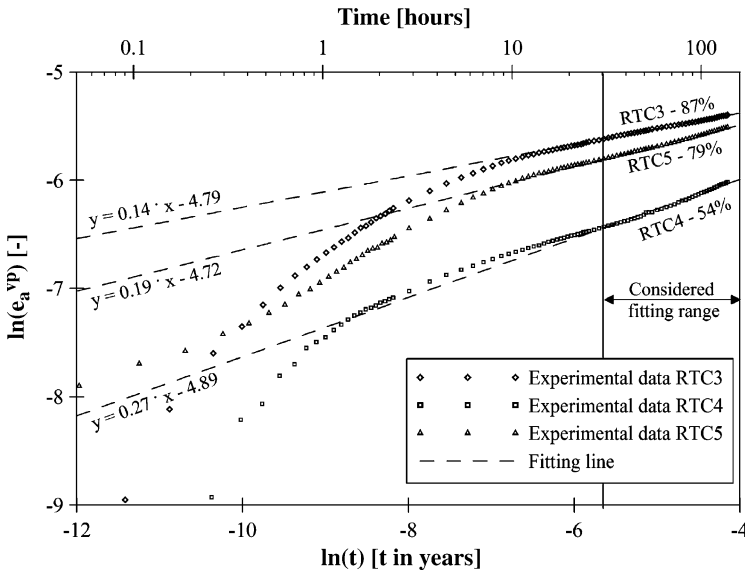


Fig. 13. Procedure for the evaluation of parameters  $\alpha_i$  for the VIPLA model

**Table 6.** Parameters of VIPLA model for the Raticosa tunnel at laboratory scale (stress in kPa and time in years)

$E$ (kPa)	$19.2 \times 10^3$
$\nu$	0.3
$\gamma$	$1.13 \times 10^{-28}$
$m$	-3.91
$n$	7.14
$a$	$2.85 \times 10^{-06}$
$\alpha$	0.20
$\beta$	1.45

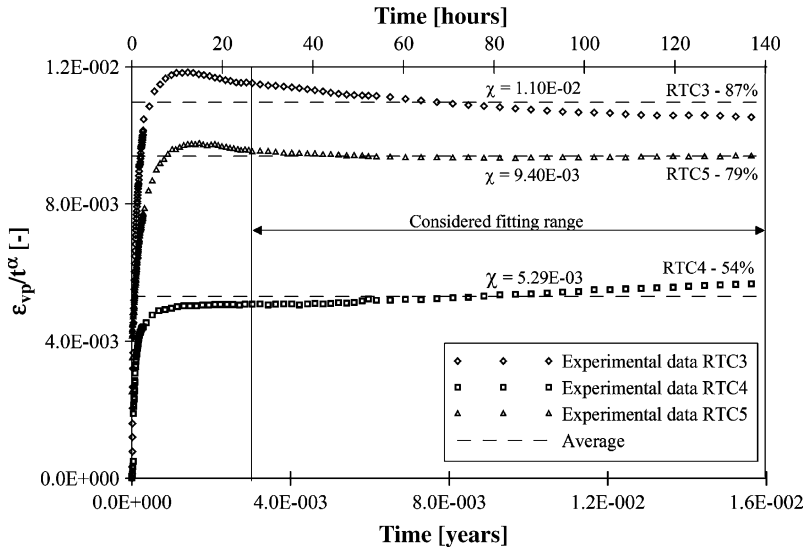


Fig. 14. Procedure for the evaluation of parameters  $\chi_i$  for the VIPLA model

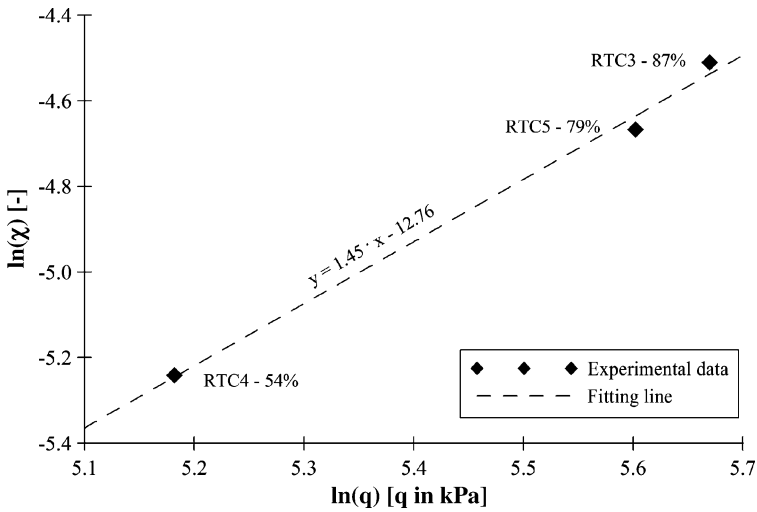
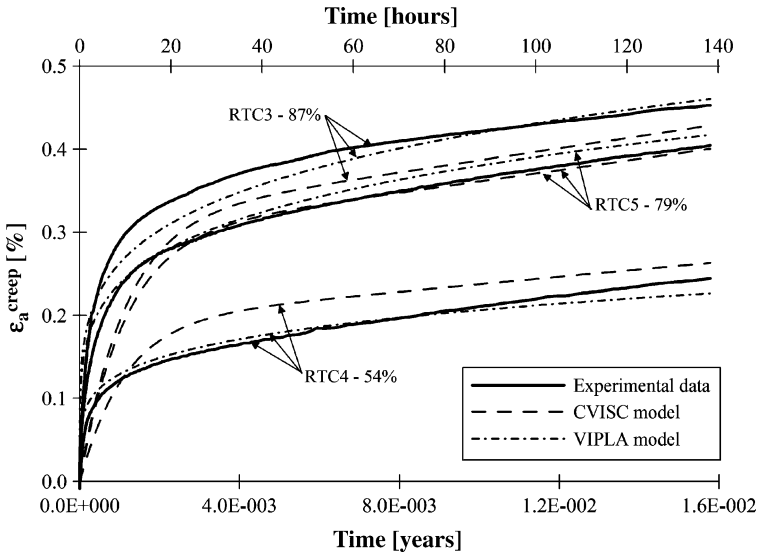


Fig. 15. Procedure for the evaluation of parameters  $\beta$  and  $a$  for the VIPLA model

according to Eq. (24). Figures 14 and 15 illustrate the computational steps performed for CS; the corresponding parameters are given in Table 6.

### 4.3 Discussion

A comparison between the experimental data of triaxial creep tests and the results of numerical computations, carried out using both the CVISC model and the VIPLA



**Fig. 16.** Comparison between experimental data and numerical analysis performed using CVISC and VIPLA models

model, is shown in Fig. 16. In either case the agreement is good. The VIPLA model is found to reproduce better than the CVISC model the shape of the creep curve, especially in its first part, and the dependency of the visco-plastic strain on the deviatoric stress.

## 5. Case Study

The Raticosa tunnel is one of the most significant underground works along the Bologna-Florence high-speed railway line (Lunardi and Focaracci, 1999). This 10.5 km long tunnel crosses the CS (through a length of 5.5 km), a marly formation and an arenaceous formation (Fig. 1).

The tunnel at the North portal has been excavated through a landslide area, formed of intensely tectonised Clay Shales, under a limited overburden (from a few meters to 100 m). The landslide is active with displacement rates ranging from more than 4 mm/year to 0–1.5 mm/year, with obvious implications on the tunnel response during and following excavation.

The tunnel (14 m span, 160 m<sup>2</sup> cross-section), excavated full face (Fig. 17) with a fibre-glass dowel reinforcement of the face and a heavy support system installed at the heading, underwent significant extrusion of the tunnel face. A detailed monitoring programme was adopted during tunnel excavation thus providing a data-base of radial convergence of the tunnel and extrusion of the tunnel face.

The construction stage consisted of excavation (in steps of 1.5 m length approximately), followed by immediate installation of heavy steel sets (every meter) embedded in shotcrete. The final lining invert was cast within a distance of about one tunnel diameter from the face and the length of each cast segment was generally 11 m.



Fig. 17. Raticosa tunnel full face excavation (courtesy of Rocksoil, Milano)

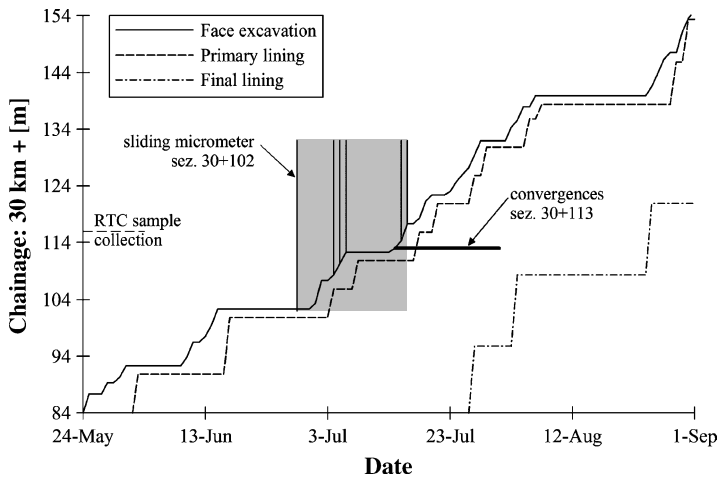
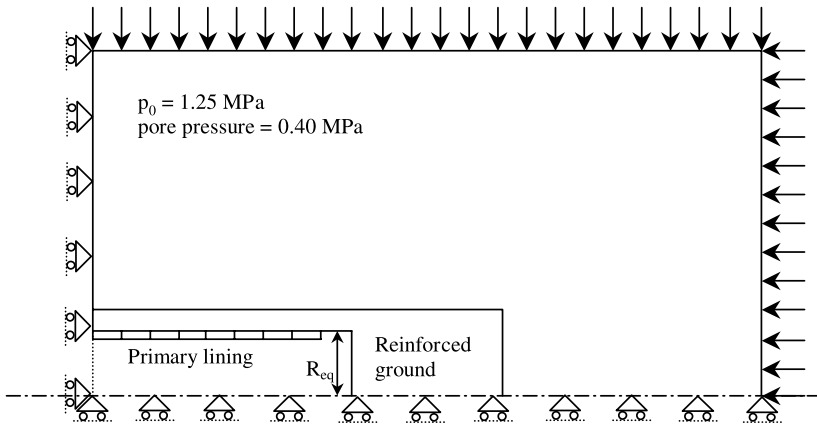


Fig. 18. Detail of the construction-excitation sequence

Finally, the concrete lining was completed at about 30–40 m behind the face. Figure 18 shows the detail of the construction-excitation sequence.

Numerical analyses were performed using the finite difference method and the Flac code (Itasca, 2001). Axis-symmetric models were adopted (Fig. 19) which reproduce the full excavation sequence of an equivalent circular tunnel ( $R_{eq} = 7$  m) at a depth of 50 m (initial state of stress  $p_0 = 1.25$  MPa, pore pressure 0.40 MPa). The reinforcement was represented by a core annulus ahead of the face with increased parameters, while the support was simulated with a 0.3 m-thick circular elastic ring (elastic modulus  $E = 29000$  MPa, Poisson's ratio  $\nu = 0.2$ ). The models did not include the final lining. The excavation sequence used in the numerical models during ad-



**Fig. 19.** Boundary and initial conditions of the numerical models

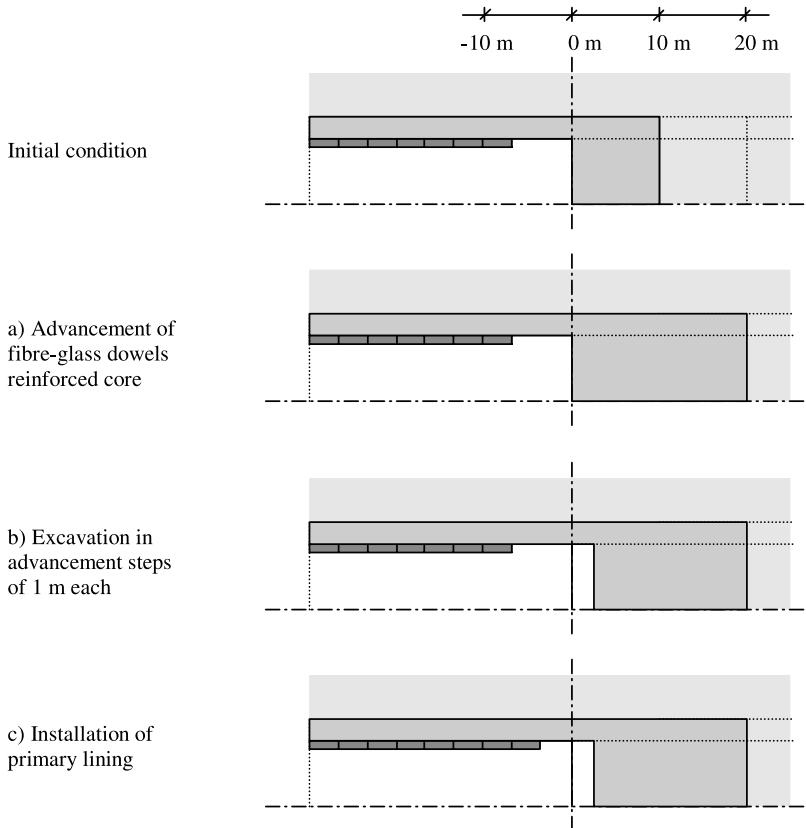


**Fig. 20.** Modelling of construction-excitation sequence

vancement is shown in Fig. 20. According to the low permeability of the CS, as determined during laboratory tests, the analyses were performed in undrained conditions.

With consideration given to the time-dependent behaviour, as observed during laboratory testing and in situ monitoring, the numerical analyses were performed by using the CVISC and VIPLA models. Different computational procedures for the simulation of face advancement were used depending on the tunnel excavation.

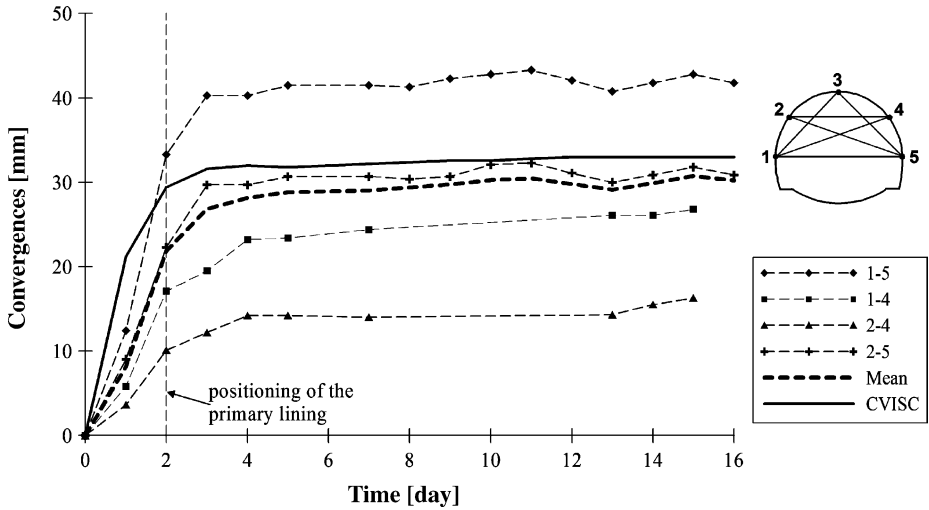


Fig. 21. Comparison between numerical results and monitoring data: radial convergence of the tunnel at chainage 30 km + 113 m (CVISC model)

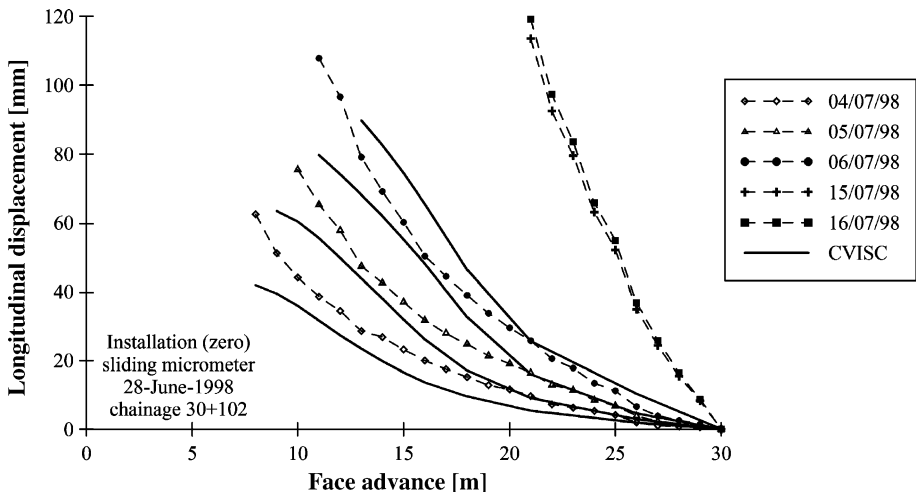


Fig. 22. Comparison between numerical results and monitoring data: extrusion of the tunnel face, chainage 30 km + 102 m (CVISC model)

Preliminary analyses, carried out with the CVISC model, demonstrated that this does not reproduce the tunnel response satisfactorily if the constitutive parameters derived from laboratory tests are used. Then, a series of parametric analyses were performed in order to evaluate these parameters at the tunnel scale. To reduce the computation time, a simplification was introduced in the model and a constant average rate of advancement of 1 m/day simulated, without considering the advancement stops.

The results obtained with the parameters of the CVISC model shown in Table 5 are illustrated in Figs. 21 and 22, where the computed values are compared with the

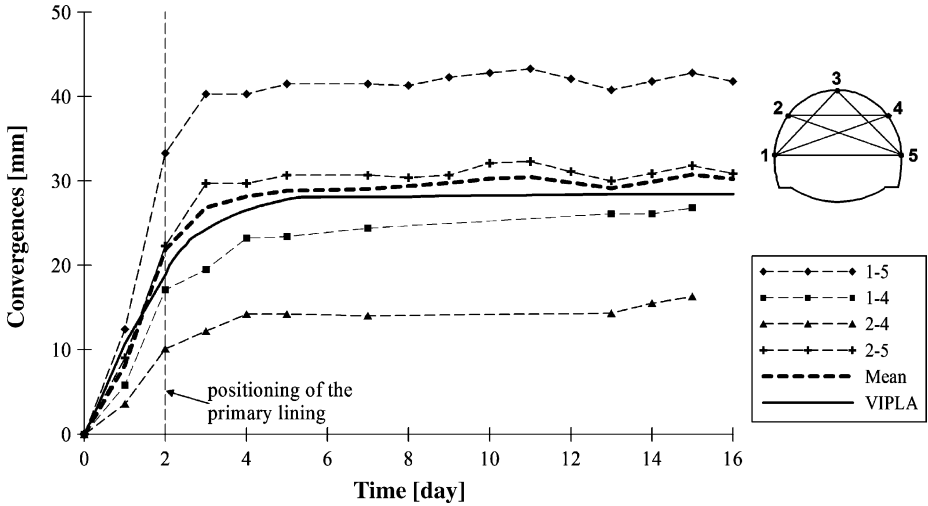


Fig. 23. Comparison between numerical results and monitoring data: radial convergence of the tunnel at chainage 30 km + 113 m (VIPLA model)

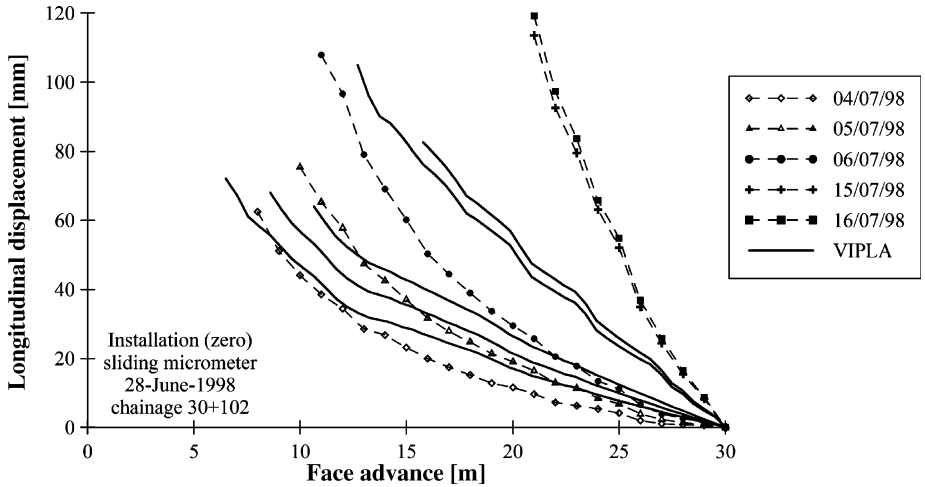


Fig. 24. Comparison between numerical results and monitoring data: extrusion of the tunnel face, chainage 30 km + 102 m (VIPLA model)

monitored data. It is shown that the CVISC model represents reasonably well the mean tunnel convergence and the extrusion of the tunnel face, except for the 15 and 16 July data. The disadvantage lies in the need to scale-up the parameters with respect to the laboratory values.

Different from the CVISC model, the analyses performed with the VIPLA model show that the monitored data can be well reproduced by using the parameters determined at laboratory scale. In this case, the excavation-construction sequence is simulated in detail, according to the time schedule shown in Fig. 18. With the laboratory visco-plastic parameters given in Table 2, and the same elastic parameters of the CVISC model ( $E = 1000 \text{ MPa}$ ,  $\nu = 0.3$ ), the results illustrated in Figs. 23 and 24 are obtained.

It is shown again that the mean tunnel convergence versus time is well reproduced (Fig. 23). As far as the extrusion of the tunnel face the agreement is rather good for the July 4 and 5 sets of measurements, as it becomes less satisfactory for the July 6, 15 and 16 data.

The response in terms of tunnel convergence (Figs. 21 and 23) is quite similar for the two models. However, the primary lining exhibits a softer behaviour with the CVISC model. With reference to the longitudinal displacements (Figs. 22 and 24), a difference is to be found in the shape of the curves. The CVISC model leads to “smooth” curves while a slope change can be noticed in the VIPLA response, whenever a stop of face advancement takes place.

## 6. Conclusions

The studies carried out on the Apennines Clay Shales (CS) in order to describe their time-dependent behaviour at laboratory and tunnel scale have been described in this paper. The interest has been posed on the geotechnical characterisation of specimens taken at the face of the Raticosa tunnel. It has been shown that the time-dependent behaviour of CS cannot be neglected and a constitutive law accounting for elastic, plastic and viscous components of behaviour need be adopted in modelling.

Two constitutive laws appear to be adequate for the description of the mechanical behaviour: a visco-elastic plastic model (CVISC) accounting for the Mohr-Coulomb yield criterion and the elastic visco-plastic Lemaitre’s model (VIPLA). In fact, the elasto-plastic constitutive laws do not reproduce the full range of behaviour of the tunnel. Based on fitting of the experimental data at laboratory scale, the constitutive parameters have been determined for each model.

Numerical analyses performed on axis-symmetric finite difference models have shown that the ground response at the tunnel face and in its surrounding can be described in detail. In particular, the same set of parameters has been used both at laboratory and at tunnel scale for the VIPLA model; on the contrary, the CVISC model required parameter scaling in order to match the monitoring data. The role of time-dependent constitutive laws in the analysis of tunnels during full face excavation has been underlined.

Based on the present work, the following conclusions can be drawn: (a) the time-dependent behaviour of CS is a significant factor to be taken under close consideration for the assessment of the tunnel response to excavation; (b) laboratory testing is necessary in order to determine the relevant features of the mechanical behaviour of the

material, however the parameters determined from laboratory tests cannot be always directly used for appropriate prediction of tunnel behaviour; (c) monitoring is essential for the assessment of the tunnel response (stability of the face and of the core ahead of the face), including the effectiveness of the stabilization measures and of the primary lining, and the time of its installation.

### Acknowledgements

The work described in this paper was carried out with the financial support of the Italian Ministry for University and Research (M.I.U.R.) as part of the Research Programme “Mechanised excavation of tunnels” (40%), co-ordinated by G. Barla. The authors are very grateful to Dr. Giovanna Cassani of Rocksoil, Milano, for providing the monitoring data of the Raticosa tunnel.

### References

- A.G.I. (1979): Some Italian experiences on the mechanical characterization of structurally complex formations. In: Proc. 4th Int. Congr. on Rock Mechanics, Montreux, France.
- Alonso, E. E., Vaunat, J., Gens, A. (1999): Modelling the mechanical behaviour of expansive clays. *Eng. Geol.* 54, 173–183.
- Anagnostou, G. (1991): Untersuchungen zur Statik des Tunnelbaus in quellfähigem Gebirge. Dissertation N. 9553. ETH. Zurich, Switzerland.
- Anagnostou, G. (1995): Seepage flow around tunnels in swelling rock. *Int. J. Numer. Anal. Met.* 19, 705–724.
- Aristorenas, G. V. (1992): Time-dependent behaviour of tunnels excavated in shale. Ph.D. Thesis, Massachusetts Institute of Technology, Boston, USA.
- Barla, G. (2001): Tunnelling under squeezing rock conditions. In: Kolymbas, D. (ed.) *Tunnelling mechanics*. Eurosummer School, Innsbruck, pp 169–268.
- Barla, G. (2006): Large size tunnels excavated full face in difficult conditions. In: Löw, S. (ed.) *Geologie und Geotechnik der Basistunnels am Gottherd und am Löttschberg*, pp 275–286.
- Barla, G., Pazzagli, G., Rabagliati, U. (1986): The San Donato tunnel (Florence). In: Proc. Int. Congress on Large Caverns, pp 61–69.
- Barla, G., Forlati, F., Zaninetti, A. (1990): Prove di laboratorio su rocce tenere: problematiche ed esempi. In: Barla, G. (ed.) *Terzo Ciclo di Conferenze di Meccanica e Ingegneria delle Rocce, MIR90*. SGEEditoriali, Padova.
- Barla, G., Barla, M., Bonini, M. (2004): Characterisation of Italian clay shales for tunnel design. *Int. J. Rock Mech. Min. Sci.* 41(3). CD-ROM, © 2004 Elsevier Ltd.
- Barla, M. (1999): Tunnels in swelling ground – simulation of 3D stress paths by triaxial laboratory testing. Ph.D. Thesis, Politecnico di Torino, Italy.
- Bellwald, P. (1990): A contribution to the design of tunnels in argillaceous rock. Ph.D. Thesis, Massachusetts Institute of Technology, Boston, USA.
- Boidy, E. (2002): Modélisation numérique du comportement différé des cavités souterraines. Ph.D. Thesis, Université Joseph Fourier, Grenoble, France.
- Boldini, D. (2002): Deep tunnels in weak rock-masses: analysis of the ground-shotcrete interaction. Ph.D. Thesis, University of Rome La Sapienza, Italy.

- Bonini, M. (2003): Mechanical behaviour of Clay-Shales (Argille Scagliose) and implications on the design of tunnels. Ph.D. Thesis, Politecnico di Torino, Italy.
- Bonini, M., Barla, M., Barla, G. (2003): Characterisation studies of tectonized Clay Shales and implications in the excavation of large size tunnels. In: Proc. 10th Int. Congr. on Rock Mechanics – ISRM 2003, Johannesburg.
- Bultel, F. (2001): Prise en compte du gonflement des terrains pour le dimensionnement des revêtements des tunnels. Ph.D. Thesis. Ecole Nationale des Ponts et Chaussées, Paris, France.
- Burland, J. B. (1990): On the compressibility and shear strength of natural clays. *Géotechnique* 40(3), 329–378.
- Cicoiella, A., Picarelli, L. (1990): Decadimento meccanico di una tipica argilla a scaglie di elevata plasticità. *Ital. Geotechnical J.* 24, 5–23.
- D’Elia, B. (1980): Processi di ammorbidimento di un’argilla marnosa con struttura a scaglie. In: Proc., XIV Geotechnical National Congress, Vol. 2, pp 409–418.
- D’Elia, B. (1991): Deformation problems in the Italian structurally complex clay soils. In: Proc., 10th Europ. Conf. on Soil Mech. and Found. Eng., Vol. 4, pp 1159–1170.
- Di Maio, C., Fenelli, G. B. (1997): Clayey soil deformability: the influence of physico-chemical interactions. *Ital. Geotechnical J.* 1, 43–54.
- Einstein, H. H. (2000): Tunnels in Opalinus Clayshale – a review of case histories and new developments. *Tunn. Undergr. Sp. Tech.* 15(1), 13–29.
- Gioda, G., Cividini, A. (2002): Numerical methods for the analysis of tunnel performance in squeezing rocks. *Rock Mech. Rock Engng.* 29(4), 171–193.
- Grob, H. (1972): Anhydrite Schwelldruck in Belchentunnel. *Int. Symp. on Underground Openings.* Lucerna, Switzerland, pp 99–119.
- Gysel, M. (2002): Anhydrite dissolution phenomena: three case-histories of anhydrite karst caused by water tunnel operation. *Rock Mech. Rock Engng.* 35(1), 1–21.
- Huder, J., Amberg, G. (1970): Soft Quellung in mergel, Opalinuston und anhydrit. *Schweizerische Bauzeitung* 88(43), 975–980.
- Itasca Inc. (2001): Flac2D 3.3, User’s manual. Minneapolis, USA.
- Lemaitre, J., Chaboche, J. L. (1996): *Mécanique des matériaux solides.* Dunod, pp 253–341.
- Leroueil, S., Vaughan, P. R. (1990): The general and congruent effects of structure in natural soils and weak rocks. *Géotechnique* 40(3), 467–488.
- Loret, B., Hueckel, T., Gajo, A. (2002): Chemo-mechanical coupling in saturated porous media: elastic-plastic behaviour of homoionic expansive clays. *Int. J. Solids Struct.* 39, 2773–2806.
- Lunardi, P., Focaracci, A. (1999): The Bologna to Florence high speed railway line: progress of underground. In: Alten et al. (eds) *Challenges of the 21st Century*, Balkema, Rotterdam.
- Madsen, F. T. (1999): Suggested methods for laboratory testing of swelling rocks. *Int. J. Rock Mech. Min. Sci. Geomech. Abstr.* 26(3), 211–225.
- Mitchell, J. K., Soga, K. (2005): *Fundamentals of soil behaviour*, 3rd edn. John Wiley and Sons Inc., Hoboken, New Jersey, USA.
- Olszak, W., Perzyna, P. (1964): On Elastic/Viscoplastic Soils, *Rhéologie et Mécanique des sols.* Symposium Franco-Polonais, Grenoble, Springer-Verlag, pp 47–57.
- Pellet, F., Hajdu, A., Deleruyelle, F., Besnus, F. (2005): A viscoplastic constitutive model including anisotropic damage for the time dependent mechanical behaviour of rock. *Int. J. Numer. Anal. Meth. Geomech.* 29, 941–970.

- Perzyna, P. (1966): Fundamental problems in viscoplasticity. *Advances in applied mechanics*, Vol. 9, Academic Press, pp 243–377.
- Picarelli, L., Olivares, L. (1998): Ingredients for modelling the mechanical behaviour of intensely fissured clay shales. In: *The geotechnics of hard soils – soft rocks*. Balkema, Rotterdam, pp 771–770.
- Picarelli, L., Olivares, L., Di Maio, C., Urciuoli, G. (2000): Properties and behaviour of tectonized clay shales in Italy. In: *The geotechnics of hard soils – soft rocks*. Balkema, Rotterdam, 1211–1241.
- Pimentel, E. (1996): Quellverhalten von diagenetisch verfestigtem Tonstein. Ph.D. Thesis, Karlsruhe, Germany.
- Pregl, O., Fuchs, M., Müller, H., Petschl, G., Riedmüller, G., Schwaighofer, B. (1980): Dreiaxiale Schwellversuche an Tongesteinen. *Geotechnik* 3, 1–7.
- Wittke, W. (1978): Grundlagen für die Bemessung und Ausführung von Tunnels in quellendem Gebirge und ihre Anwendung beim Bau der Wendeschleife der S-Ban Stuttgart. Veröff. Institut f. Grundbau, Bodenmech, Felsmech., Verkehrswasserbau, RWTH Aachen, 6 pp.
- Wittke, W. (2000): Swelling stability analysis for tunnels – fundamentals. Verlag Glückauf GmbH, Essen, Germany.
- Wong, R. C. K. (1998): Swelling and softening of La Biche shale. *Can. Geotech. J.* 35, 206–221.

**Author's address:** Dr. M. Bonini, Politecnico di Torino, DISTR-Corso Duca degli Abruzzi 24, 10129 Torino, Italy; e-mail: mariacristina.bonini@polito.it